Exactly solvable antiferromagnetic Blume-Capel model on a sawtooth chain

Yan-Ping Guo, Zhong-Qiang Liu, Yu-Liang Xu, and Xiang-Mu Kong*
College of Physics and Engineering, Qufu Normal University, Qufu 273165, China
(Received 12 January 2016; published 31 May 2016)

The geometrically frustrated spin-1 Blume-Capel model on an infinite sawtooth chain is exactly solved by the transfer matrix method. The magnetization, ground-state phase diagram, magnetocaloric properties, and specific heat of the system are investigated. The results indicate that: (i) Magnetization plateaus appear at zero temperature. Their number depends on the sign of the crystal field D. For $D \geqslant 0$ there are two magnetization plateaus; however, for $D < 0$ five plateaus exist. At a finite temperature, thermal excitation will destroy these plateaus completely. (ii) Phase transition between any two long-range-ordered ground states, whose spin configurations are given in phase diagram, is the first-order one. The macroscopic degeneracy of the ground states described by the entropy only exists at phase coexistence points. (iii) As temperature approaches zero, magnetocaloric properties and entropy change sharply near phase coexistence points. (iv) The crossovers of the specific heat from a single-peak structure to double-peak ones can signal the phase coexistence points in ground-state phase diagram.

DOI: 10.1103/PhysRevE.93.052151

I. INTRODUCTION

Geometrically frustrated spin systems (GFSS) [1] exhibit many interesting and intriguing phenomena in both experimental and theoretical investigations (see Ref. [2] and references therein). An antiferromagnetic model on a regular lattice, in which all elementary (minimal) closed contours are formed by odd number of sites, provides a good theoretical platform to depict and investigate these phenomena of GFSS. A very simple but nontrivial example is the antiferromagnetic model on the sawtooth chain with a topology of corner-sharing triangles (see Fig. 1). The sawtooth chain exists in some magnetic compounds, such as the delafossite $YCuO_{2.5+x}$ [3,4] and the olivines ZnL_2S_4 (L = Er, Tm, Yb) [5]. Despite of oversimplification to some extent, this model has attracted a considerable amount of attention [6,7], since it may capture a number of important features of real systems [8–11], such as a double-peak structure of the specific heat. Recently, although some exact solutions of the low-dimensional spin-1/2 GFSS [12–18] have been reported, it is still an open issue to exactly describe the thermodynamics of the sawtooth chain with higher spins.

The spin-1 Blume-Capel (BC) model [19,20] plays a crucial role in both statistical mechanics and condensed matter physics. Crystal field D (sometimes named as the single-ion anisotropy parameter) within this model is an important parameter that may affect the system's critical properties. As a typical paradigm in the standard Ising universality class [21], the BC model has been intensively studied on bipartite lattices [22–29], in which the sign of the exchange coupling J is irrelevant to their critical properties in the absence of the external field. However, an antiferromagnetic BC model ($J < 0$) on nonbipartite lattices may display different behaviors qualitatively [30–36]. The frustrated antiferromagnetic spin-1 BC model on a triangular lattice has been investigated by renormalization group method [37] and transfer matrix method [38], respectively. It is found that finite-temperature antiferromagnetic long-range order accompanying with multicritical phenomena appears within a certain range of the crystal field D strength. For the frustrated Ising models with spin-1/2, it takes a long time to investigate whether long-range-ordered ground states (LROGS) exist in these systems [39–43]. Besides the frustrated antiferromagnetic BC model, little work studying on LROGS of spin-1 BC model has been reported. Thus, to deeply understand the basic properties of various GFSS, it is worthwhile to find out the exact solutions of the related systems. Recently, exact solutions of spin-1/2 antiferromagnetic Ising and Ising-like models were obtained [44,45]. To the best of our knowledge, the thermodynamics of the geometrically frustrated BC model on a sawtooth chain has not been exactly solved.

Therefore, the motivation for the present work was to solve the geometrically frustrated antiferromagnetic BC model on a sawtooth chain by the transfer matrix method. We will mainly focus on the magnetic properties and specific heat of the system. Our results indicate that the system exhibits several magnetization plateaus at zero temperature. These plateaus are associated with different LROGS, which depend on the sign of the crystal field D. Each phase transition presented on the ground-state phase diagram is the first-order one. As to the specific heat, it exhibits a crossover from a double-peak structure to a single-peak one as the parameters (crystal field and magnetic field) approach the phase coexistence point (PCP).

The rest of paper is organized as follows. In Sec. II, the antiferromagnetic BC model on a sawtooth chain is introduced, and then its exact solution is derived by the transfer matrix method. In Sec. III, the magnetic properties and the ground-state phase diagram are analyzed. In Sec. IV, the magnetocaloric properties and the specific heat are studied in detail. Conclusion is given in Sec. V.

II. MODEL AND METHOD

The antiferromagnetic spin-1 Blume-Capel model on an infinite sawtooth chain in an external magnetic field H is schematically shown in Fig. 1. Obviously, the coordination numbers of each top site and underline one are 2 and 4,

*kongxm@mail.qfnu.edu.cn

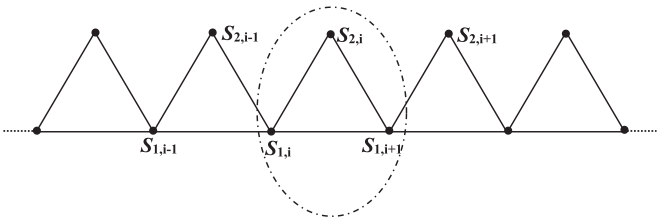

FIG. 1. Antiferromagnetic BC model on an infinite sawtooth chain. Sites that belong to two different sublattices (top and bottom) are denoted as $s_{1,i}$ and $s_{2,i}$, respectively.

respectively. Thus, the model's Hamiltonian reads

$$\mathcal{H} = -J\sum_i (s_{1,i}s_{2,i} + s_{1,i}s_{1,i+1} + s_{2,i}s_{1,i+1}) - D\sum_i \left(s_{1,i}^2 + s_{2,i}^2\right) - H\sum_i (s_{1,i} + s_{2,i}), \quad (1)$$

where $J < 0$ is the antiferromagnetic exchanging parameter between two nearest-neighbor spins, D is the crystal field, $s_{1,i}$, $s_{2,i} = \pm 1, 0$. In Eq. (1), the first sum runs over all the nearest-neighbor spin pairs, the second and the third sums run over all the spin sites.

According to the conventional method in statistical physics to deal with thermodynamics problems, the system's partition function should be obtained first. By introducing the free energy, some thermodynamic parameters, such as magnetization and specific heat, may be expressed by it and its partial derivatives. The partition function of the model defined by Eq. (1) reads

$$Z = \sum_{s_1}\sum_{s_2} e^{-\beta\mathcal{H}} = \sum_{s_1}\sum_{s_2} \exp\Big[K\sum_i \times (s_{1,i}s_{2,i} + s_{1,i}s_{1,i+1} + s_{2,i}s_{1,i+1}) + d\sum_i \left(s_{1,i}^2 + s_{2,i}^2\right) + h\sum_i (s_{1,i} + s_{2,i})\Big], \quad (2)$$

where $\beta = 1/(k_B T)$, k_B is the Boltzmann constant, T is the thermodynamics temperature, $K = \beta J$, $d = \beta D$, and $h = \beta H$. The sum over s_1 and s_2 in Eq. (2) means the summations over all possible spin configurations on the lattice.

As mentioned above, our aim is to investigate the BC model on an infinite sawtooth chain. To achieve this goal, we first assume that there are $2N$ sites on the sawtooth chain. $s_{1,i}$, $s_{2,i}$, and $s_{1,i+1}$ in a triangle consist of the ith block; see Fig. 1. Thus, the chain may be divided into N blocks. In order to ensure that the system obeys the translational symmetry, we adopt the periodic boundary conditions (cyclic conditions); i.e., $s_{1,N+i} = s_{1,i}$ and $s_{2,N+i} = s_{2,i}$. Naturally, the infinite sawtooth chain may be obtained as $N \to \infty$. Because Hamiltonians of different blocks are commutative, one can expand the exponent in Eq. (2) and get the product of the terms corresponding to different blocks; i.e.,

$$Z = \sum_{s_1}\prod_{i=1}^{N}\sum_{s_2=-1,0,1} \exp\Big[K(s_{1,i}s_{2,i} + s_{1,i}s_{1,i+1} + s_{2,i}s_{1,i+1}) + d\left(\frac{s_{1,i}^2 + s_{1,i+1}^2}{2} + s_{2,i}^2\right) + h\left(\frac{s_{1,i} + s_{1,i+1}}{2} + s_{2,i}\right)\Big]. \quad (3)$$

Equation (3) shows that the trace for each block can be calculated separately. The sum in Eq. (3) over all states of spin s_2 in each block can be obtained independently from the others. It yields

$$Z = \sum_{s_1}\prod_{i=1}^{N}(z_1 + z_2 + z_3), \quad (4)$$

where

$$z_1 = \exp\big[-K(s_{1,i} - s_{1,i}s_{1,i+1} + s_{1,i+1}) + d\left(s_{1,i}^2 + s_{1,i+1}^2 + 2\right)/2 + h(s_{1,i} + s_{1,i+1} - 2)/2\big],$$
$$z_2 = \exp\big[Ks_{1,i}s_{1,i+1} + d\left(s_{1,i}^2 + s_{1,i+1}^2\right)/2 + h(s_{1,i} + s_{1,i+1})/2\big],$$
$$z_3 = \exp\big[K(s_{1,i} + s_{1,i}s_{1,i+1} + s_{1,i+1}) + d\left(s_{1,i}^2 + s_{1,i+1}^2 + 2\right)/2 + h(s_{1,i} + s_{1,i+1} + 2)/2\big].$$

After applying the periodic boundary conditions to Eq. (4), it can be written in the standard transfer matrix form

$$Z = \mathrm{Tr}V^N, \quad (5)$$

where V is the transfer matrix,

$$V = \begin{pmatrix} w_{11} & w_{12} & w_{13} \\ w_{21} & w_{22} & w_{23} \\ w_{31} & w_{32} & w_{33} \end{pmatrix}. \quad (6)$$

Here,

$$w_{11} = \exp(-K+2d) + \exp(K+d+h) + \exp(3K+2d+2h),$$
$$w_{12} = \exp[-K+(3d-h)/2] + \exp[(d+h)/2] + \exp[K+3(d+h)/2],$$
$$w_{13} = \exp(-K+2d-h) + \exp(-K+d) + \exp(-K+2d+h),$$
$$w_{21} = \exp[-K+(3d-h)/2] + \exp[(d+h)/2] + \exp[K+3(d+h)/2],$$
$$w_{22} = \exp(d-h) + 1 + \exp(d+h),$$
$$w_{23} = \exp[K+3(d-h)/2] + \exp[(d-h)/2] + \exp[-K+(3d+h)/2],$$
$$w_{31} = \exp(-K+2d-h) + \exp(-K+d) + \exp(-K+2d+h),$$
$$w_{32} = \exp[K+3(d-h)/2] + \exp[(d-h)/2] + \exp[-K+(3d+h)/2],$$
$$w_{33} = \exp(3K+2d-2h) + \exp(K+d-h) + \exp(-K+2d).$$

Equations (5) and (6) mean that the partition function can be written in the form of the sum of the Nth power of the eigenvalues λ_i ($i = 1,2,3$) of the transfer matrix, namely,

$$Z = \sum_{i=1}^{3}\lambda_i^N. \quad (7)$$

Since the characteristic equation of Eq. (6) is a third-order polynomial equation, it may have three real eigenvalues, or one real eigenvalue together with two complex conjugate eigenvalues. It is easy to obtain their analytical expressions. Numerical analysis show that the transfer matrix Eq. (6) always has three real eigenvalues and one is always larger than the

other two. Let λ_1 be the largest eigenvalue and its explicit expression is

$$\lambda_1 = \frac{a}{3} + \frac{1}{3}\left[\left(\frac{b+3\sqrt{3c}}{2}\right)^{1/3} + \left(\frac{b-3\sqrt{3c}}{2}\right)^{1/3}\right], \quad (8)$$

where

$$\begin{aligned} b &= 2a^2 + 9ap + 27q, \\ c &= 4a^3q + 18apq + 27q^2 - a^2p^2 - 4p^3, \\ a &= w_{11} + w_{22} + w_{33}, \\ p &= w_{12}w_{21} + w_{13}w_{31} + w_{23}w_{32} - w_{11}w_{22} \\ &\quad - w_{22}w_{33} - w_{33}w_{11}, \\ q &= w_{11}w_{22}w_{33} + w_{12}w_{23}w_{31} + w_{13}w_{21}w_{32} \\ &\quad - w_{11}w_{23}w_{32} - w_{12}w_{21}w_{33} - w_{13}w_{22}w_{31}. \end{aligned}$$

In the limit $N \to \infty$, it can be proved that the partition function is completely determined by the largest eigenvalue λ_1 itself, namely,

$$Z = \lambda_1^N, \quad N \to \infty. \quad (9)$$

For further analysis, we introduce the free energy per site $f = -\ln Z/(2N\beta)$. Its expression is

$$f = -\frac{\ln \lambda_1}{2\beta}. \quad (10)$$

Combining Eq. (10) with Eq. (8), one can obtain the analytical expression of f. As mentioned above, once the analytical expression of f is derived, one can immediately use it to investigate the other physical quantities, such as the magnetization, magnetocaloric properties, and specific heat, which are defined as the corresponding partial derivatives of the free energy, respectively. In the following sections, we shall focus on these properties of the model. From these analytical expressions, we investigate the magnetic properties and spin configurations of the ground states of BC model on an infinite sawtooth chain.

III. MAGNETIZATION AND THE GROUND STATES

A. Magnetization

The magnetization per site is given by the following relation:

$$m \equiv -\left(\frac{\partial f}{\partial H}\right)_T = \frac{1}{2\lambda_1}\frac{\partial \lambda_1}{\partial h}. \quad (11)$$

To obtain the second relation in Eq. (11), Eq. (10) and the relation $h = \beta H$ were used. Inserting Eq. (8) into Eq. (11), one can directly obtain the corresponding explicit expression of the magnetization m. However, its expression is too cumbersome to be presented here.

For different $D/|J|$, the total magnetization as a function of the external magnetic field H for several values of the reduced temperature $k_BT/|J|$ are shown in Fig. 2. Figure 2 exhibits that at low temperature (e.g., $k_BT/|J| = 0.01$), magnetization shows three typical behaviors for different values of $D/|J|$. Moreover, the magnetization curves exhibit several magnetization plateaus, which are quite reminiscent of the zero-temperature magnetization plateaus (corresponding to LROGS at zero temperature). It is noteworthy that the true magnetization plateaus and magnetization jumps appear just at zero temperature (see an example in Fig. 6), while the magnetization is continuous at any finite temperature even though low-enough temperature. Figure 2 indicates that, due to the effect of thermal fluctuation, the magnetization plateaus vanish quickly as temperature increases.

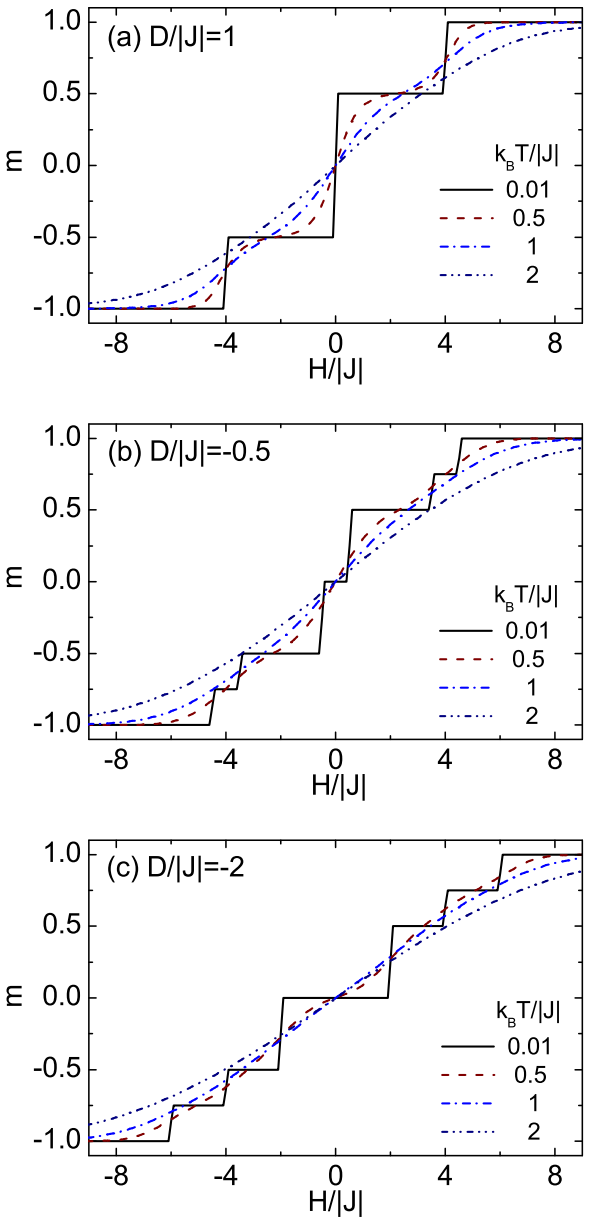

FIG. 2. The total magnetization per site as a function of the external magnetic field for various values of the reduced temperature. (a) $D/|J| = 1$, (b) $D/|J| = -0.5$, (c) $D/|J| = -2$.

According to the aforementioned discussion on the magnetization plateau, we can get some important properties of the ground states from low-temperature data. At low temperature, for $D/|J| > 0$, there are two magnetization plateaus with $m = \pm 0.5$ [see Fig. 2(a)]. Positive D tends to drive the spin locating at $+1$ or -1 state. As $|H|$ decreases, effect of antiferromagnetic interaction becomes evident. That is to say, each fourth spin reverse, the system exhibits its antiferromagnetic property.

$|m|$ decreases from 1 to 0.5. However, for $D/|J| < 0$, there are five magnetization plateaus with $m = 0, \pm 0.5, \pm 0.75$ [see Figs. 2(b) and 2(c)]. As $|H|$ decreases, negative D and frustration effect tend to drive part of spins locating at 0 state. The competition among negative D, antiferromagnetic interaction, and H results in more ground states than those in the case of $D/|J| > 0$.

Figure 2 exhibits that the temperature plays an important role in affecting the magnetization and existence of the LROGS. To clearly illustrate its effect, for $D/|J| = 1, -0.5, -2$, Fig. 3 plots the total magnetization curves versus $k_BT/|J|$ with several different $H/|J|$. Since m is an odd function of $H/|J|$ (i.e., $m(k_BT/|J|, D/|J|, H/|J|) = -m(k_BT/|J|, D/|J|, -H/|J|)$), it is sufficient to restrict our discussion to the positive values of $H/|J|$. In general, m decreases with increasing temperature because the thermal fluctuation weakens the magnetization. However, as $T \to 0$, all magnetization curves converge to the same asymptotic limit provided the magnetic field is selected within the stability range of a given magnetization plateau (LROGS), while the special asymptotic limit of exactly one curve corresponds to a PCP of the first-order phase transition. As mentioned in the above paragraph, the number of the LROGS depends on $D/|J|$. For $D/|J| = 1$, there are four LROGS and three PCPs. For $D/|J| = -0.5$ or -2, there are seven LROGS and six PCPs. One can also obtain the same results from Fig. 4.

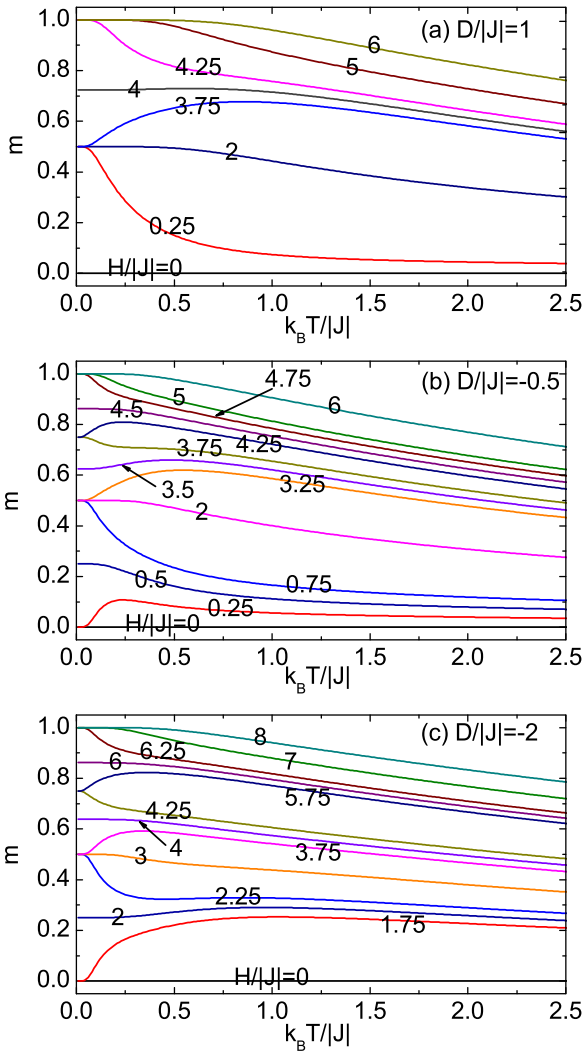

FIG. 3. The total magnetization per site as a function of the reduced temperature for various values of the external magnetic field $H/|J|$. (a) $D/|J| = 1$, (b) $D/|J| = -0.5$, (c) $D/|J| = -2$.

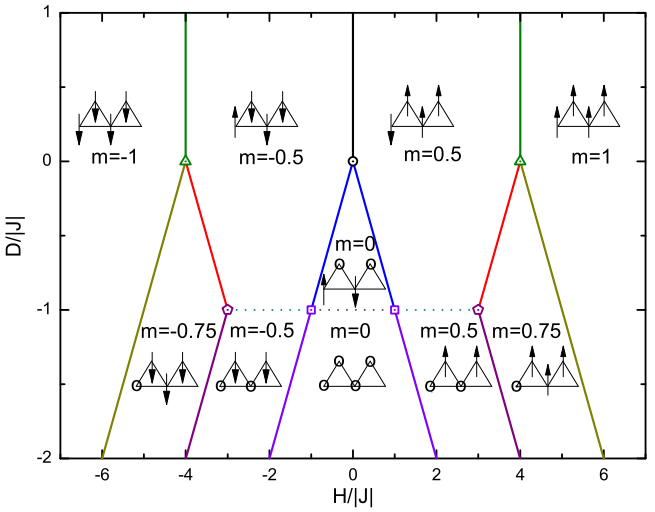

FIG. 4. Ground-state phase diagram. The phase coexistence curves divides the phase diagram into ten regions. Each region corresponds with a long-range-ordered ground state, whose corresponding configuration is given in the inset. The symbol "↑," "o," or "↓" on each lattice point represents the state $+1$, 0, or -1 of the corresponding spin, respectively.

B. Ground-state phase diagram

Having the explicit expression for the total magnetization per site Eq. (11), it is possible to perform an exact analysis of the magnetization properties of all ground states, i.e., the system's spin configurations at $T = 0$. The ground-state phase diagram with spin configurations is shown in Fig. 4.

Figure 4 shows that there are ten jointed regions in the plane of $H/|J|$ versus $D/|J|$. These regions indicate that the system has ten LROGS with the magnetization $m = 0, \pm 0.5, \pm 0.75$, and ± 1, respectively. The infinite sawtooth chain can be divided into lots of periodic element cell with four spins, as shown in the insets of Fig. 4. The symbol "↑," "o," or "↓" on each lattice point represents the state $+1$, 0, or -1 of the corresponding spin, respectively. Figure 4 exhibits that at $T = 0$ positive D tends to drive the spin locating at $+1$ or -1 state; nevertheless, negative D and frustration effect tend to drive part of spins locating at 0 state, which agrees well with the results shown in Fig. 2. The lines and their joints (indicated by triangle, square, pentagon, or circle) represent the phase coexistence lines and PCPs of the model, respectively. The horizontal dot lines divide the different spin configurations with the same m.

According to Eq. (11), all the approximate numerical values of the PCPs' magnetization may be calculated. They are shown in Fig. 5. Take a phase transition line (the dark yellow dash dot line in Fig. 5) from $m = 1$ to 0.75 for example, its approximate numerical value is $m \approx 0.861803$, which was obtained by the

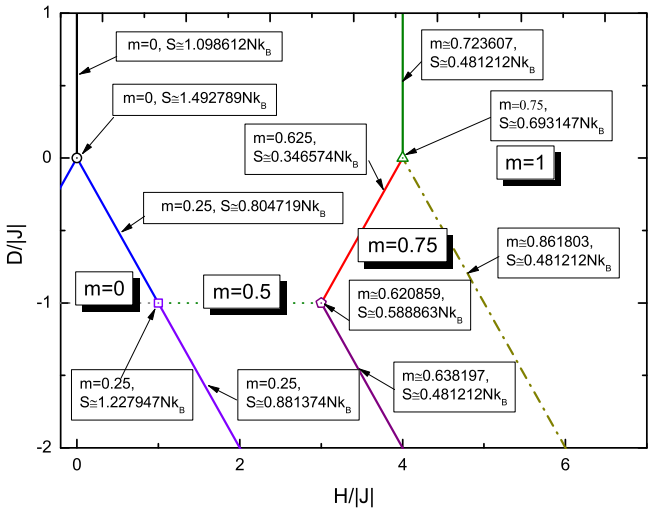

FIG. 5. The values of the magnetization and entropy at PCPs.

following exact expression of the magnetization:

$$m = (3 + 1/\sqrt{5})/4. \tag{12}$$

Inserting the relation $D/|J| = -H/|J| + 4$ into Eq. (11), and then finding its asymptotic limit as $T \to 0$, one can obtain Eq. (12). The rest of the exact values of m can be derived by the same way. To keep the text concise, they are given in the Appendix.

As expected, the magnetization of PCP is different from its adjacent LROGS. To clearly illustrate the differences between the magnetizations of the LROGS and those of the PCPs, we plot the total magnetization as a function of H for $D/|J| = -1$ at zero temperature (see Fig. 6). Obviously, the LROGS and the PCPs have different magnetization. Moreover, from Fig. 6 one may find that the system must undergo a PCP in each phase

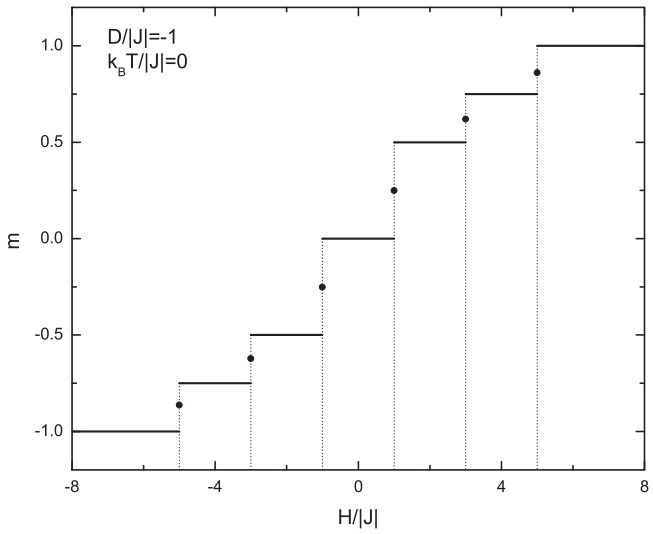

FIG. 6. The magnetization of the model as a function of the external magnetic field for $T = 0$ and $D/|J| = -1$. The values of magnetization at PCPs $(H/|J|, D/|J|) = (\mp 5, -1)$, $(\mp 3, -1)$, and $(\mp 1, -1)$ are $m \approx \mp 0.861803$, $m \approx \mp 0.620859$, and $m = \mp 0.25$, respectively.

transition from one LROGS to another. Thus, these transitions are first-order phase transitions.

C. The degeneracy of the ground state

On the one hand, phase coexistence exists at discontinuous phase transition lines and PCPs. It leads to a nontrivial macroscopic degeneracy of the ground states. The macroscopic degeneracy may be described by the entropy S of the entire system,

$$S = k_B \ln \Omega. \tag{13}$$

On the other hand, from Eq. (10) the entropy of the present model, which consists of $2N$ sites, is given as follows:

$$S = -2N \frac{\partial f}{\partial T} = N k_B \left[\ln \lambda_1 + T \frac{\partial (\ln \lambda_1)}{\partial T} \right]. \tag{14}$$

Inserting Eq. (8) into Eq. (14), one can directly obtain the analytical expression of the entropy S. However, it is too cumbersome to be presented here. Employing the expression of the entropy and the same method used in obtaining magnetization, one can calculate the entropy S for the PCP.

Figure 5 presents all the numerical values of the entropy S (in units of Nk_B) for each PCP. It is found that their values approach to infinite as $N \to \infty$. Combining these results with Eq. (13), we know that the degree of degeneracy of each PCP is infinite. Figure 5 shows that three completely different phase boundaries with $m \approx 0.861803$, 0.723607, and 0.638197 have the same value of the entropy. This phenomenon can be interpreted as that all those phase boundaries belong to the universality class of the hard-dimer model and the magnetization values are different just because either down or zero spin state are replaced with the notion of the hard dimers [46,47]. However, there is merely one state configuration for each LROGS. Thus, there is no degeneracy. Naturally, the system's entropy is zero at LROGS.

IV. THERMAL PROPERTIES OF THE MODEL

A. Magnetocaloric properties

Recently, it has been demonstrated that several frustrated spin systems may exhibit an enhanced magnetocaloric effect during the adiabatic demagnetization, which might be of practical importance for low temperature magnetic refrigeration [48–50]. This fact stimulates us to investigate the magnetocaloric properties of BC model on an infinite sawtooth chain. Using Eq. (11) and thermodynamic Maxwell equation, we can obtain the isothermal magnetic entropy change per spin:

$$\Delta S = \int_0^H \left(\frac{\partial m}{\partial T} \right)_H dH. \tag{15}$$

To explore the magnetocaloric properties of the model, we first present response of the magnetization to the change of temperature in a constant magnetic field. As shown in Fig. 7(a), the most distinct changes of $(\frac{\partial m}{\partial T})_H$ appear only near the field-induced phase transitions, while almost no changes can be seen within the respective plateaus. The phenomenon reflects that at low temperature the thermal fluctuation cannot destroy the LROGS far away from the PCPs, but it plays an important role in varying m from a LROGS to another across a PCP.

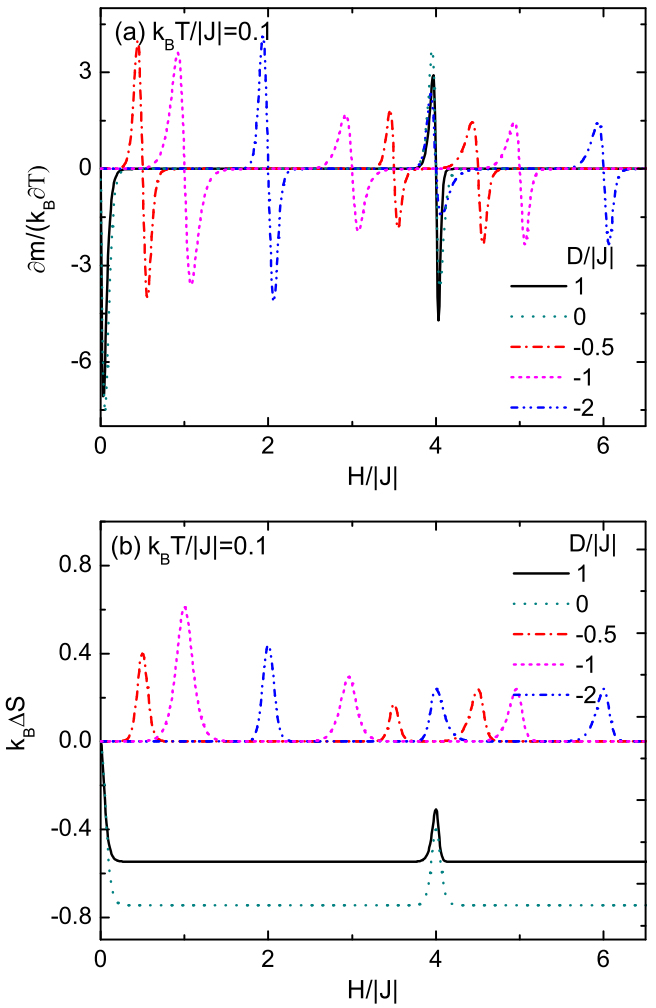

FIG. 7. (a) Field-dependence of the derivative of magnetization with respect to temperature at constant field for $k_BT/|J| = 0.1$. (b) Field-dependence of the isothermal entropy change for $k_BT/|J| = 0.1$.

This behavior of the magnetization response to the change of temperature may be translated into the magnetic entropy change ΔS, as evidenced in Fig. 7(b). Combining Fig. 4 with Fig. 7(b), one can find the physical reason for the different behaviors of curves with different signs of $D/|J|$. For $D/|J| \geqslant 0$, the system is in a state of phase coexistence in absence of a magnetic field. As the magnetic field H increases, $\Delta S < 0$. For $D/|J| < 0$, the system is in a LROGS when $H = 0$. As H increases, $\Delta S \geqslant 0$. Obviously, the most distinct magnetocaloric effect can be detected only around the PCPs as H approaches the values of transition magnetic field. With the external field augmenting, the increase of ΔS can be explained in terms of the low-lying thermal excitation arising from a LROGS without degeneracy to a PCP with infinite degree of degeneracy, and vice versa. In the former case the system cools down and in the latter case it heats up when the external magnetic field is augmented adiabatically.

B. Specific heat

Last but not least, let us explore in detail the specific heat per site of the model. From the free energy Eq. (10), the specific heat per site is given directly by the largest eigenvalue λ_1, namely,

$$c(T) = -T\left(\frac{\partial^2 f}{\partial T^2}\right)_H = \frac{k_B T}{2}\left\{2\frac{\partial(\ln\lambda_1)}{\partial T} + T\frac{\partial^2(\ln\lambda_1)}{\partial T^2}\right\}. \quad (16)$$

In fact, the dependency behavior of the specific heat on the temperature exhibits similar characteristics near different PCPs. Here we only give two typical examples. For $D/|J| = -2$ and 1 the overall characteristics of the specific heat as a function of the temperature for several magnetic fields $H/|J|$ are shown in Figs. 8(a)–8(d), respectively. At PCPs $[(D/|J|,\ H/|J|) = (-2,2),\ (1,4)]$ the specific heat exhibits a broad peak, which is a common feature of the one-dimensional antiferromagnetic quantum spin system [51]. When the parameters leave away from the PCPs in any direction, the specific heat exhibits double-peak structure. Besides the aforementioned broad peak, a rather sharp peak at a lower temperature appears. As the parameters change further, the specific heat broadens and exhibits merely a single peak. The above analysis indicates that the crossovers of specific heat from single-peak behavior to double-peak ones can signal the PCPs in ground-state phase diagram.

Similar double-peak structures of the heat specific have been discussed on several systems previously [8,11,12]. For spin-1/2 GFSS on a finite sawtooth chain, both the triplet and the singlet first excited states converge to the exactly dispersionless excited states with an identical energy in the thermodynamic limit [8]. Comparing Fig. 8 in this paper with Fig. 3 in Ref. [8], one may conjecture that energies of a higher-energy singlet and a lower-lying doublet split from a triplet (the lowest excitation of spin-1 antiferromagnetic BC model with single-ion anisotropy [52,53]) also converge to the same limiting value as $N \to \infty$. These excited states lead to a sharp peak of the specific heat at a low temperature [8].

V. CONCLUSION

In this paper, geometrically frustrated BC model on an infinite sawtooth chain was investigated by the transfer matrix technique exactly. By deriving the analytical expression of the largest eigenvalue of the transfer matrix, we studied the system's magnetization, ground-state phase diagram, magnetocaloric properties, and specific heat, subsequently. Our results indicate that:

(i) The true magnetization plateaus and magnetization jumps appear just at zero temperature. The number of the magnetic plateaus depends on the sign of the single-ion anisotropy D. When $D/|J| \geqslant 0$, five magnetization plateaus with $m = \pm 0.75, \pm 0.5$, and 0 appear as a consequence of the frustration. When $D/|J| < 0$, only two magnetization plateaus $m = \pm 0.5$ appear. At a very low temperature, magnetization plateaus are quite reminiscent of the zero-temperature magnetization plateaus. As temperature increases further, due to the effect of thermal fluctuation, the magnetization plateaus vanish quickly.

(ii) As one of the main results of the present paper, the spin configurations of all the LROGS and PCPs are shown in the ground-state phase diagram. All phase transitions are the first-order ones.

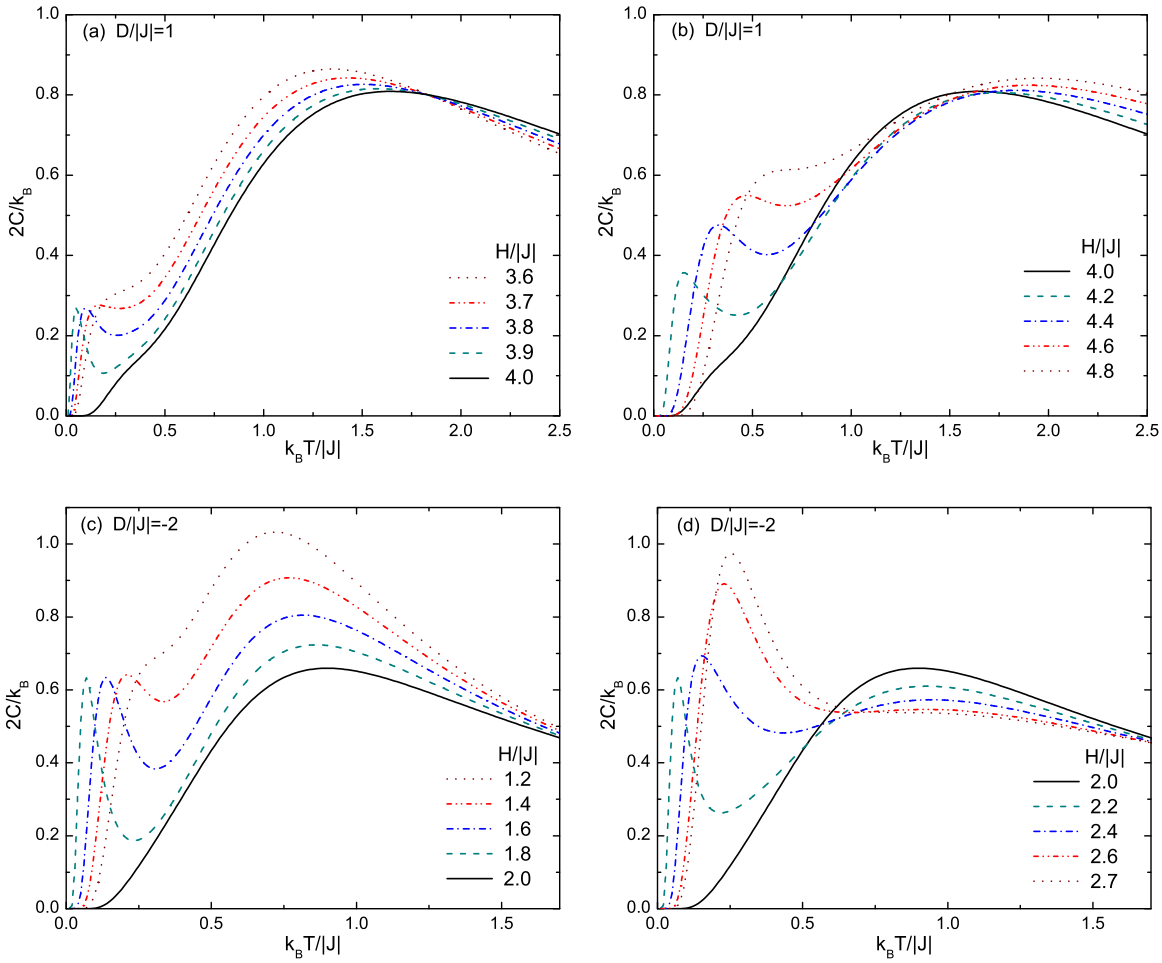

FIG. 8. Temperature-dependence of the specific heat for several values of the external field $H/|J|$. (a) $D/|J| = 1$, $H/|J| \leqslant 4.0$; (b) $D/|J| = 1$, $H/|J| \geqslant 4.0$; (c) $D/|J| = -2$, $H/|J| \leqslant 2.0$; (d) $D/|J| = -2$, $H/|J| \geqslant 2.0$.

(iii) As temperature approaches zero, magnetocaloric properties and entropy change sharply near PCPs. The degree of macroscopic degeneracy of the ground states described by the entropy merely exists at PCPs.

(iv) When the parameters approaches any PCP, the specific heat will exhibit a double-peak structure. Besides the broad peak, a rather sharp peak at a lower temperature appears. At PCP, only the broad peak exists. Thus, the crossovers of the specific heat from a single-peak structure to double-peak ones can signal the PCPs in ground-state phase diagram.

The present investigation only considered the nearest-neighbor interaction of the model. However, it is also worthwhile to remark that the exactly solved spin-1 Ising sawtooth chain can be substantially generalized to account for the next-nearest-neighbor interaction and the multispin interaction, etc. Therefore, our future effort will focus on these aspects.

ACKNOWLEDGMENTS

This work is supported by the National Natural Science Foundation of China (Grants No. 11275112 and No. 11302118), the Shandong Natural Science Foundation (Grant No. ZR2013AQ015), and the Science Foundation of Qufu Normal University (Grants No. BSQD2012053 and No. xkj201305). Y.-P. Guo thanks E. Jurcisinova for valuable correspondence and Chun-Yang Wang, Ze-Guo Ren, Xiao-Jie Li, and Xiao-Ming Ma for fruitful discussions and useful comments.

APPENDIX: THE EXACT VALUES OF THE MAGNETIZATION

For the phase transition line between the LROGS with $m = 1$ and that with $m = 0.5$ (the olive line in Fig. 5), the exact value of the magnetization is

$$m = (1 + 1/\sqrt{5})/2.$$

Its approximate value is 0.723607.

For two phase transition lines between the plateau with $m = 0.75$ and that with $m = 0.5$ (the red line and the purple one in Fig. 5), the magnetization has two typical values for various values of $D/|J|$. For $-1 < D/|J| < 0$, the exact value of magnetization at any PCPs is

$$m = 5/8.$$

For $D/|J| < -1$, the exact value of magnetization at any PCPs is

$$m = (3 - 1/\sqrt{5})/4.$$

Its approximate value is 0.638197.

For the phase transition line between the plateau with $m = 0.5$ and that with $m = 0$ (the violet line and the blue one in Fig. 5), the exact value of the magnetization at any PCPs is

$$m = 1/4.$$

At the PCPs $(H/|J|, D/|J|) = (1, -1)$, (4,0), and $(3, -1)$, the values of the total magnetization per site are, respectively,

$$m = 1/4,$$

$$m = 3/4,$$

and

$$m = \frac{1}{2} + \frac{1}{\sqrt{21}}\cos(\theta/3),\ \theta = \pi - \arctan(\sqrt{3}/9).$$

Its approximate value is 0.620859.

[1] G. Toulouse, Commun. Phys. **2**, 115 (1977).
[2] J. E. Greedan, J. Mater. Chem. **11**, 37 (2001).
[3] R. J. Cava, H. W. Zandbergen, A. P. Ramirez, H. Takagi, C. T. Chen, J. J. Krajewski, W. F. Peck Jr., J. V. Waszczak, G. Meigs, R. S. Roth, and L. F. Schneemeyer, J. Solid State Chem. **104**, 437 (1993).
[4] O. Le Bacq, A. Pasturel, C. Lacroix, and M. D. Núñez-Regueiro, Phys. Rev. B **71**, 014432 (2005).
[5] G. C. Lau, B. G. Ueland, R. S. Freitas, M. L. Dahlberg, P. Schiffer, and R. J. Cava, Phys. Rev. B **73**, 012413 (2006).
[6] J. Richter, J. Schulenburg, A. Honecker, J. Schnack, and H.-J. Schmidt, J. Phys.: Condens. Matter **16**, S779 (2004).
[7] O. Derzhko, A. Honecker, and J. Richter, Phys. Rev. B **76**, 220402(R) (2007).
[8] K. Kubo, Phys. Rev. B **48**, 10552 (1993).
[9] T. Nakamura and K. Kubo, Phys. Rev. B **53**, 6393 (1996).
[10] S. A. Blundell and M. D. Núñez-Regueiro, Eur. Phys. J. B **31**, 453 (2003).
[11] V. Elser, Phys. Rev. Lett. **62**, 2405 (1989).
[12] J. Strečka, M. Jaščur, M. Hagiwara, K. Minami, Y. Narumi, and K. Kindo, Phys. Rev. B **72**, 024459 (2005).
[13] L. Čanová, J. Strečka, and M. Jaščur, J. Phys.: Condens. Matter **18**, 4967 (2006).
[14] J. S. Valverde, O. Rojas, and S. M. de Souza, J. Phys.: Condens. Matter **20**, 345208 (2008).
[15] M. S. S. Pereira, F. A. B. F. de Moura, and M. L. Lyra, Phys. Rev. B **77**, 024402 (2008).
[16] M. S. S. Pereira, F. A. B. F. de Moura, and M. L. Lyra, Phys. Rev. B **79**, 054427 (2009).
[17] D. Antonosyan, S. Bellucci, and V. Ohanyan, Phys. Rev. B **79**, 014432 (2009).
[18] V. Ohanyan, Condens. Matter Phys. **12**, 343 (2009).
[19] M. Blume, Phys. Rev. **141**, 517 (1966).
[20] H. W. Capel, Physica **32**, 966 (1966); **33**, 295 (1967); **37**, 423 (1967).
[21] N. G. Fytas, Eur. Phys. J. B **79**, 21 (2011).
[22] E. H. Graf, D. M. Lee, and J. D. Reppy, Phys. Rev. Lett. **19**, 417 (1967).
[23] M. Blume, V. J. Emery, and R. B. Griffiths, Phys. Rev. A **4**, 1071 (1971).
[24] J. Lajzerowicz and J. Sivardière, Phys. Rev. A **11**, 2079 (1975); J. Sivardière and J. Lajzerowicz, *ibid.* **11**, 2090 (1975); **11**, 2101 (1975).
[25] A. K. Jain and D. P. Landau, Phys. Rev. B **22**, 445 (1980); B. L. Arora and D. P. Landau, AIP Conf. Proc. **10**, 870 (1973).
[26] D. M. Saul, M. Wortis, and D. Stauffer, Phys. Rev. B **9**, 4964 (1974).
[27] A. N. Berker and M. Wortis, Phys. Rev. B **14**, 4946 (1976).
[28] T. W. Burkhardt and H. J. F. Knops, Phys. Rev. B **15**, 1602 (1977); T. W. Burkhardt, *ibid.* **14**, 1196 (1976).
[29] A. F. Siqueira and I. P. Fittipaldi, Physica A **138**, 592 (1986).
[30] M. Kaufman and M. Kanner, Phys. Rev. B **42**, 2378 (1990).
[31] I. Puha and H. T. Diep, J. Magn. Magn. Mater. **224**, 85 (2001).
[32] V. O. Özçelik and A. N. Berker, Phys. Rev. E **78**, 031104 (2008).
[33] O. D. Rodriguez Salmon and J. R. Tapia, J. Phys. A **43**, 125003 (2010).
[34] A. Malakis, A. N. Berker, I. A. Hadjiagapiou, N. G. Fytas, and T. Papakonstantinou, Phys. Rev. E **81**, 041113 (2010).
[35] M. Žukovič and A. Bobák, Phys. Rev. E **87**, 032121 (2013).
[36] E. Aydiner and C. Akyüz, Chin. Phys. Lett. **22**, 2382 (2005).
[37] G. D. Mahan and S. M. Girvin, Phys. Rev. B **17**, 4411 (1978).
[38] J. B. Collins, P. A. Rikvold, and E. T. Gawlinski, Phys. Rev. B **38**, 6741 (1988).
[39] G. H. Wannier, Phys. Rev. **79**, 357 (1950).
[40] R. R. P. Singh and D. A. Huse, Phys. Rev. Lett. **68**, 1766 (1992).
[41] J. Villian, R. Bidaux, J.-P. Carton, and R. Conte, J. Phys. **41**, 1263 (1980).
[42] W. F. Wolff and J. Zittartz, Z. Phys. B **49**, 229 (1982).
[43] J. Strečka and J. Čisárová, Physica A **392**, 5633 (2013).
[44] J. Strečka, O. Rojas, T. Verkholyak, and M. L. Lyra, Phys. Rev. E **89**, 022143 (2014).
[45] B. Lisnyi and J. Strečka, J. Magn. Magn. Mater. **377**, 502 (2015).
[46] J. Richter, Low Temp. Phys. **31**, 695 (2005).
[47] O. Derzhko and J. Richter, Eur. Phys. J. B **52**, 23 (2006).
[48] M. E. Zhitomirsky, Phys. Rev. B **67**, 104421 (2003).
[49] A. Honecker and S. Wessel, Physica B **378**, 1098 (2006).
[50] J. Schnack, R. Schmidt, and J. Richter, Phys. Rev. B **76**, 054413 (2007).
[51] J. C. Bonner and M. E. Fisher, Phys. Rev. **135**, A640 (1964).
[52] F. D. M. Haldane, Phys. Lett. A **93**, 464 (1983); Phys. Rev. Lett. **50**, 1153 (1983).
[53] J. P. Renard, M. Verdaguer, L. P. Regnault, W. A. C. Erkelens, J. Rossat-Mignod, and W. G. Stirling, Europhys. Lett. **3**, 945 (1987).